

# Green Prospective Approach of Chromium Zinc Oxide Nanoparticles for Highly Ultrasensitive Electrochemical Detection of Anti-hypotensive Medication in Various Matrices

Khadejah D. Otaif, Manal M. Fouad, Noha S. Rashed, Noha Y.Z. Hosni, Ahmed Elsonbaty, and Elsayed Elgazzar\*



Cite This: *ACS Omega* 2023, 8, 30081–30094



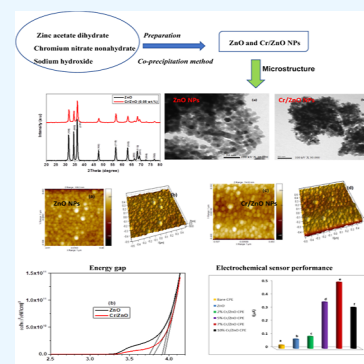
Read Online

ACCESS |

Metrics & More

Article Recommendations

**ABSTRACT:** A highly ultrasensitive sensor that relied on Cr/ZnO-NPs was developed to detect etilefrine hydrochloride (ETF) in different matrices via a particular green voltammetric technique. The X-ray diffraction pattern showed the nanomaterials of the polycrystalline hexagonal structure. The energy-dispersive X-ray spectrum approved the presence of Cr<sup>3+</sup> inside the host zinc oxide framework. The morphological and topological characteristics were visualized using transmission electron microscopy and atomic force microscopy micrographs describing the nanoparticles in spherical-like shape with large-surface area. The energy gap ( $E_g$ ) was evaluated from transmittance ( $T\%$ ) and reflectance ( $R\%$ ) spectra within the visible region. The optimization study indicated that the Cr/ZnO-NP/CPE sensor has high sensitivity, thanks to the distinctive physical and chemical properties of the fabricated electrode. A new approach showed a great selectivity for determining ETF in different matrices in the presence of other interferences like levodopa. Under optimal circumstances, the square-wave voltammetry revealed a linear response to ETF from 0.01 to 10  $\mu\text{mol L}^{-1}$  ( $r = 0.9996$ ) with quantification and detection limits of 9.11 and 2.97  $\text{nmol L}^{-1}$ , respectively. Finally, the proposed approach was effectively applied to estimate ETF in pharmaceutical dosage forms and biological fluids using simple, accurate, and selective electrochemical electrode. The greenness profile assessment of the developed method was performed using the Eco-Scale and green analytical procedure index. These tools indicated that the proposed method is an eco-friendly technique for the determination of ETF in different matrices.



## 1. INTRODUCTION

Parkinson's disease (PD) is a degenerative neurological system ailment that causes tremors, stiffness, difficulties in walking, balancing, and coordinating movement. Orthostatic hypotension (OH) is a non-motor symptom of PD that can induce unexpected falls, feebleness, dyspnea, weariness, impaired vision, and low-back discomfort while standing. It is a type of low blood pressure that occurs when you stand up suddenly from sitting or lie down. As a result, PD sufferers must take medication to keep their blood pressure in check and prevent it from plummeting. One of the most significant medications that may be used to treat OH of cardiovascular and neurological origin is etilefrine hydrochloride (ETF) which is considered as a sympathomimetic amine of the 3-hydroxy-phenylethanolamine class. Many analytical approaches for quantifying ETF in different matrices were presented. The majority of these investigations are focused on determining ETF by spectrophotometric, chemiluminescence assay, HPLC, LC-MS, and GC.<sup>1–4</sup> Despite their great accuracy and sensitivity, these techniques require expensive laboratory-based instruments, skilled technicians, tedious transportation, and storage protocols. Moreover, sample preparation procedures are

usually time-consuming, labor-intensive, and require various regular analysis processes. Otherwise, electro-analytical methods are employed in many applications because they are simple, do not require complex skills, and allow the sample to be analyzed immediately without the need for extraction.<sup>4,5</sup>

In the advanced technology, designing a developed portable electrochemical sensors is desirable for facilitating the task of monitoring as well as saving time and effort.<sup>6,7</sup> Detection sensitivity can be improved by developing an efficient electrode using more sensitive electrochemical methods such as square-wave voltammetry (SWV). SWV is a pulse voltammetry technique that is characterized by its high-speed analysis, sensitivity, and selectivity.<sup>8,9</sup> SWV sensors have low detection limit which are widely used for estimation of variety of drugs

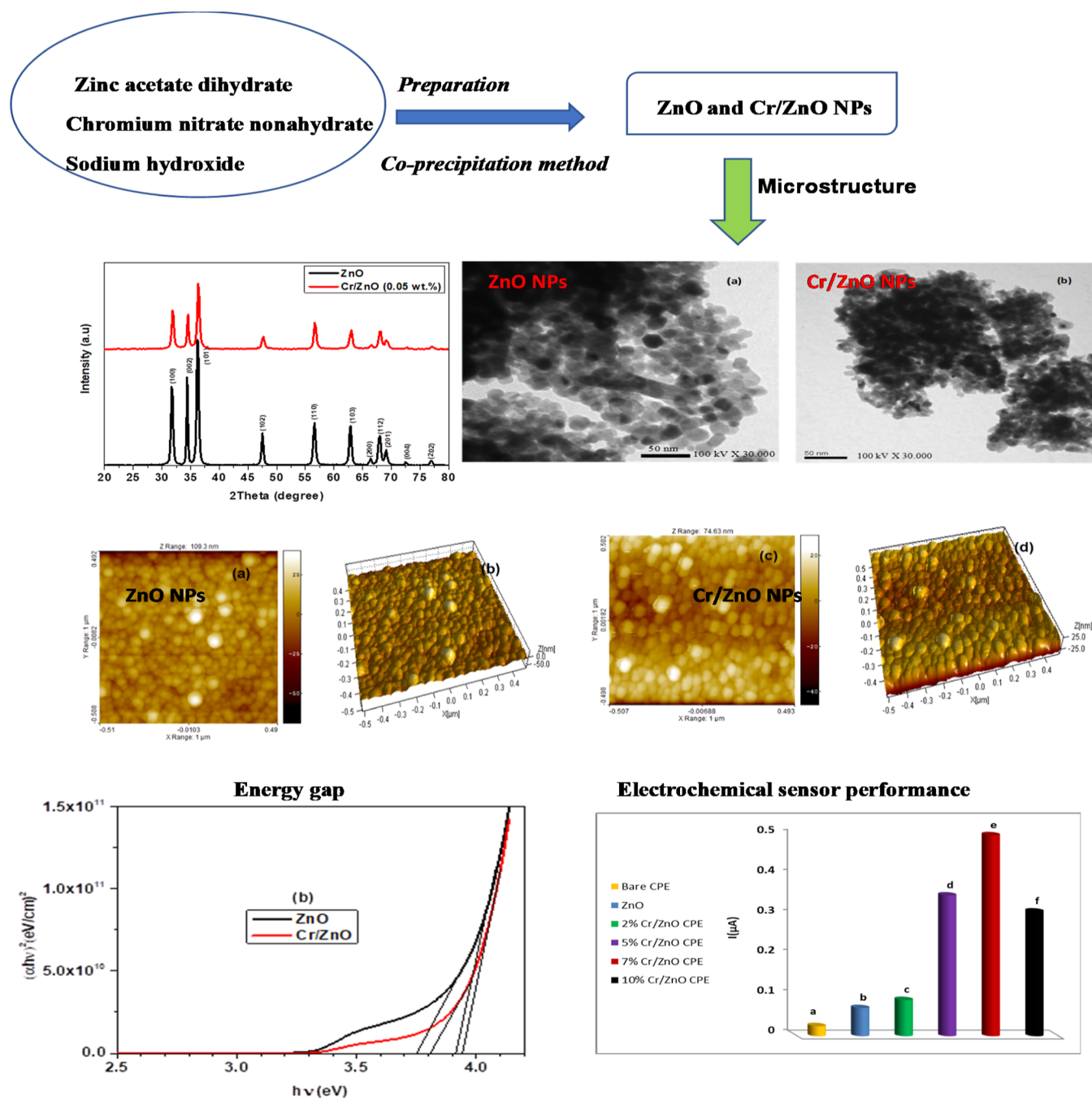
Received: April 11, 2023

Accepted: June 30, 2023

Published: August 9, 2023



### Scheme 1. Green Prospective Approach of Chromium Zinc Oxide Nanoparticles for Highly Ultrasensitive Electrochemical Detection of Anti-hypertensive Medication



with high accuracy. Furthermore, the carbon paste electrode (CPE) is frequently used as a working electrode in electrochemical analysis owing to its low background current, ease of preparation, regeneration, low cost, compatibility with a wide range of modifier types, and ohmic resistance compared to other solid electrodes.<sup>10–12</sup> On the other way, the nanotechnology was introduced as a new strategy for improvement in the electrochemical sensor performance. Nanomaterials have recently been applied in tremendous sectors comprising food processing, novel fabric chemicals, agricultural production, and therapeutics. In this regard, metal oxide semiconductors composed of binary or ternary nanoparticles (NPs) such as MnO, MgO, CuO, RuO<sub>2</sub>, TiO<sub>2</sub>, SnO<sub>2</sub>, Ce/CuO, Ag/

ZnO, Pd/MnO, and Ni-doped Fe<sub>2</sub>O<sub>3</sub> have gotten a lot of interest during the past few decades based on their excellent physicochemical advantages. Transparent semiconductor zinc oxide (ZnO) when compared to other metal oxides is a superior material of low toxicity, environmental friendliness, quantum size effect, and adaptable microstructure. In addition, it has a great deal of interest due to its applications in the electronics industry and biotechnology.<sup>13–15</sup> Integration of ZnO NPs with different metals like Au, Ag, Si, Pd, La, Ru, etc. results in producing new compounds with promising features. Indeed, electronegativity, coordinate state, size, type, and amount of dopant element are essential factors which significantly have impact on quality, size, and shape of

nanocomposites. Among numerous dopants, chromium (Cr) element was taken because of the close ionic radius of  $\text{Cr}^{3+}$  (0.063 nm) to  $\text{Zn}^{2+}$  (0.074 nm) and the similar electro-negativity of Cr (1.66) to Zn (1.65). Additionally, chromium oxide ( $\text{Cr}_2\text{O}_3$ ) is a p-type semiconductor of photoluminescence quantum efficiency and antiferromagnetic property.<sup>15,16</sup> Chinnasamy and Balasubramanian have investigated the influence of chromium ions on the structural and optical aspects of ZnO nanorods for enhancement in the UV photodetection performance.<sup>17</sup>

Moreover, magnetron sputtering, hydrothermal, chemical vapor deposition, spray pyrolysis, co-precipitation, gas phase condensation, sol-gel, and cathodic electrodeposition are important techniques used to fabricate the nanomaterials. Among aforementioned methods, a scalable and cost-effective chemical co-precipitation was utilized for preparing refined homogeneous nanometal oxides.<sup>17,18</sup> The aim of the current study is to provide a sophisticated eco-friendly technique for measurement of the ETF using SWV. The method was evaluated using GAPI and the Analytical Eco-Scale methodology. Besides, it has been utilized for examining the effect of  $\text{Cr}^{3+}$  on the microstructure of ZnO for improving the performance of the chemical sensor. To the best of our knowledge, no electrochemical approach has yet been documented in the literature for the determination of ETF. For this reason, various working electrodes were fabricated; however, chromium-doped ZnO-NPs/CPE electrodes exhibited the best sensitivity and peaked current signals, especially when compared to the other sensors used in this investigation. Additionally, the CPE sensor has promising results, suggesting that the proposed sensors can selectively detect and quantify the target analyte in low concentrations in the complex matrix, permitting its potential employment for the pharmacokinetics studies in various biological fluids of either animals or human samples.<sup>9–12</sup> One of the main goals of the suggested study is to replace the most used toxic solvents with more eco-friendly and less destructive alternatives; hence, the proposed method's greenness was assessed by using the Analytical Eco-Scale methodology and green analytical procedure index (GAPI). Because of the low chromium ion percent (0.05 wt %), it was considered that Cr/ZnO-NPs are of low toxicity compared to many other nanometal oxides.<sup>18,19</sup>

## 2. EXPERIMENTAL SECTION

**2.1. Apparatus.** Voltammetric measurements were performed using a Metrohm Computrace electrochemical analyzer Model 797 VA from Metrohm, Switzerland. VA Computrace (version 1.3.) was used to validate the measurement output signal using an Ag/AgCl (3 M KCl) electrode as the reference electrode, a Cr/ZnO-NPs/CPE as the working electrode, and a platinum wire as the auxiliary electrode. A Jenway 3330 laboratory pH meter was utilized to test the pH of the method. Deionized water used in this study was obtained from a Hamilton-Aqua-Metric deionized water system. All investigations were carried out at a temperature of 25 °C. Un-doped ZnO and Cr/ZnO nanostructures were examined by the X-ray diffractometer (Rigaku Smart Lab.). Energy-dispersive X-ray analysis (EDX; ISIS300, Oxford, England) was used to define the elemental composition of the prepared materials. Transmission electron microscopy (TEM; Hitachi-H-7500, Japan) was used to visualize the shape and mean particle size. The topological nature was identified using atomic force microscopy (AFM park system, 212). An UV/vis spectrophotometer

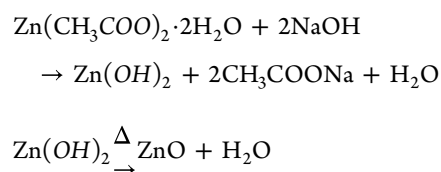
(Jasco, V-570) was employed to analyze the optical properties of the thin films (Scheme 1).

**2.2. Chemicals and Reagents.** All chemicals used within this work were of analytical grade. ETF (99.88%) and levodopa (99.44%) were provided from the National Organization for Drug Control and Research (Cairo, Egypt). Commercial formulation (Vascon) was purchased from a local pharmacy. Silicon oil (99%), zinc acetate dihydrate [ $\text{Zn}(\text{CH}_3\text{COO})_2 \cdot 2\text{H}_2\text{O}$ ,  $\geq 98\%$ ], sodium hydroxide (NaOH,  $\geq 98\%$ ), chromium nitrate nonahydrate [ $\text{Cr}(\text{NO}_3)_3 \cdot 9\text{H}_2\text{O}$ , 99%], and graphite powder (10–20  $\mu\text{m}$ ) were procured from Alfa Aesar or Merck, Germany. 100 mL of phosphate buffer solution (PBS) ( $0.1 \text{ mol L}^{-1}$ ) was prepared of  $1 \text{ mol L}^{-1}$  dipotassium phosphate ( $\text{K}_2\text{HPO}_4$ ) and  $1 \text{ mol L}^{-1}$  dihydrogen potassium phosphate ( $\text{KH}_2\text{PO}_4$ ), with a particular volume of  $0.1 \text{ mol L}^{-1}$   $\text{H}_3\text{PO}_4$  and  $0.1 \text{ mol L}^{-1}$  NaOH added for pH correction. Ethanol, acetone, and dimethyl sulfoxide solvents were obtained from El-Nasr company, Egypt. Human serum was acquired from the Zagazig University Hospital (Zagazig, Egypt) and kept frozen until use.

**2.3. Standard Solutions.** ETF stock standard solution ( $1 \text{ mmol L}^{-1}$ ) was prepared by dissolving 21.76 mg of the pure ETF in distilled water in a 100 mL volumetric flask. The solution was refrigerated till needed. A series of working solutions ( $0.01\text{--}10 \mu\text{mol L}^{-1}$ ) were prepared by the serial dilutions of the stock standard solution using PBS (0.1 M, pH 7).

### 2.4. Synthesis of Un-doped and Cr-Doped ZnO NPs.

Zinc oxide NPs were synthesized according to the chemical reaction written as



First, 6.70 g of  $\text{Zn}(\text{CH}_3\text{COO})_2 \cdot 2\text{H}_2\text{O}$  was completely dissolved in 30 mL of deionized water (1.02 mol/L) using a magnetic stirrer. After that, 2.45 g of NaOH was dissolved in 30 mL of deionized water (2.04 mol/L) and then added dropwise to aqueous zinc acetate solution with continuous stirring for 3 h at room temperature. At pH reaction  $\sim 9$ , a homogeneous white solution was formed. The precipitate powder was separated using filter paper, then washed many times by double distilled water. The resulting powder was dried at 70 °C overnight and finally annealed in a furnace oven at 400 °C for 2 h in air. Chromium doped zinc oxide (Cr/ZnO, 0.05 wt %) was synthesized by adding 0.78 g of  $\text{Cr}(\text{NO}_3)_3 \cdot 9\text{H}_2\text{O}$  (0.065 mol/L) to the starting solution with stirring for 3 h until a homogeneous white gray solution was formed. The obtained solid solution was filtered, washed, dried, and annealed at the same previous conditions.

**2.5. Working Electrodes.** Non-modified CPE was created by mixing 0.2 mL of silicon oil with 0.4 g of graphite powder using a mortar and pestle. The obtained carbon paste was poured into the electrode body's hollow and polished with filter paper until it had a shiny finish. A copper wire was used to connect the paste to the voltammetry system. Then, the ZnO NP-modified CPE was prepared by hand mixing carbon powder, binder, and 10 mg of ZnO NP with silicon oil in an agate mortar to produce a homogeneous carbon paste. The CPE electrode was designed with a geometric surface area approximately equals 3 mm diameter. The enhanced Cr/ZnO-

NPs/CPE electrode was prepared by blending 0.4 g of powdered graphite, 0.4 mL of silicon oil, and 0.044 g of Cr/ZnO-NPs/CPE powder (0.05% chromium, w/w). The electrode cavity was filled with an adequate amount of the generated paste, and the non-modified CPE operations were repeated. It is worthy to note that the fabricated electrodes are not expensive, anchored to the low cost of ZnO and Cr/ZnO (0.05 wt %) NPs as well as the cost-effective chemical technique. Here, a tiny amount of the NPs was utilized in fabricating the sensor.

**2.6. General Procedure.** A suitable amount of ETF standard solution ( $1 \text{ mmol L}^{-1}$ ) was poured in 15 mL volumetric flasks, which were then filled with PBS (0.1 M, pH 7) and thoroughly mixed to reach a final concentration of  $1 \times 10^{-4} \mu\text{mol L}^{-1}$ . Inside the voltammetric cell, the solution was agitated at 4000 rpm. During the voltammetric measurement, the stirrer was switched off for a certain period, and a specified voltage (0.4–1.2 V) was given to the modified electrode. After that, the procedure was duplicated for both CV and SWV using appropriate aliquots of ETF solution in a voltammetric cell. Finally, and most crucially, the SWV was recorded at a sweep rate of 100 mV/s, a frequency of 20 Hz, and a pulse magnitude of 20 mV.

**2.7. Applications of the Marketable Dosage Form.** In a mortar, 10 Vascon tablets (each comprising 5 mg of ETF) were correctly weighed and completely pulverized. The powder amount corresponding to two tablets (10 mg) was accurately calculated and weighted. The weighted powder was mixed with 60 mL of methanol in a 100 mL volumetric flask and sonicated for 15 min to ensure that the tablet powder dissolved evenly. Then, the flask was filled to the mark with the same solvent, making a stock solution, which was filtered using a poly(tetrafluoroethylene) (PTFE) syringe filter. Five known concentrations in the range of  $0.01\text{--}10 \mu\text{mol L}^{-1}$  were prepared by adding few  $\mu\text{L}$ s from stock solution in the specified supporting electrolyte (PBS, pH 7) and analyzed them in triplicates under comparable voltammetric conditions. ETF concentrations were recalculated using the linear regression equation relied on the standard ETF calibration curve, and recovery percentages were computed. Recovery trials were accomplished utilizing varied standard addition techniques.

**2.8. Analysis of the ETF Level in Spiked Human Serum.** Drug-free human blood samples collected from healthy volunteers from Zagazig University Hospital (Zagazig, Egypt) (after receiving their written agreement) were centrifuged for 45 min at 4000 rpm room. Then, the isolated serum samples were kept frozen until the test. Before usage, the serum samples were thawed. To assess the amount of ETF in human serum, 1 mL of serum was spiked with different volumes of therapeutic ETF, 1 mL of ethanol, and 1 mL of  $\text{ZnSO}_4$  (5%) for removing serum proteins. The serum was then centrifuged for 25 min at 14,000 rpm and filtered via a PTFE syringe filter ( $0.45 \mu\text{m}$ ). The supernatant solution (1 mL) was then added into the voltammetric cell wherein it was diluted with PBS (10 mL, pH 7). Thereafter, the developed technique was used to determine the quantity of ETF in the solution using the modified Cr/ZnO-NPs/CPE electrode. On the other hand, ZnO NPs are not toxic, and it can be used in pharmaceutical industry as well as cosmetics. Moreover, Cr/ZnO-NPs have low toxicity based on the low  $\text{Cr}^{3+}$  amount (0.05 wt %) inside the ZnO framework.

### 3. RESULTS AND DISCUSSION

**3.1. Impact of  $\text{Cr}^{3+}$  Dopants on the Microstructure Characteristics of ZnO NPs.** **3.1.1. XRD and EDX Analyses.** The X-ray diffraction (XRD) profile of un-doped and Cr-doped ZnO NPs is depicted in Figure 1. As shown, ZnO has a

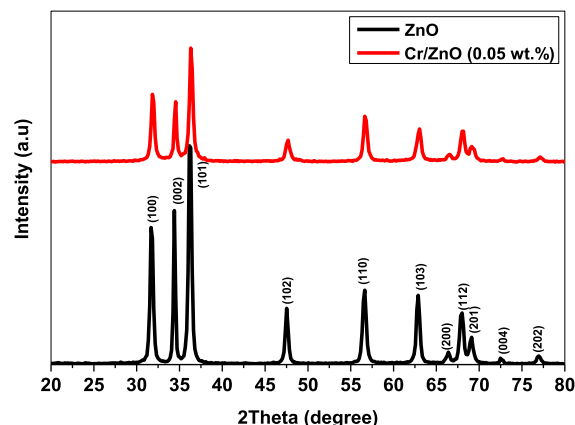


Figure 1. XRD pattern of un-doped ZnO and Cr/ZnO-NPs.

polycrystalline structure of diffraction peaks located at  $2\theta = 31.61, 34.31, 36.12, 47.36, 56.45, 62.83, 66.44, 67.97, 69.07, 72.62,$  and  $76.92^\circ$  corresponding to the reflection planes (100), (002), (101), (102), (110), (103), (200), (112), (201), (004), and (202), respectively, which are consistent with the hexagonal wurtzite structure of the standard card JCPDS no. 36-1451, space group ( $P6_3mc$ ). The sharp intensity suggests the high degree of crystallinity and big crystallite size of un-doped ZnO. However, the peaks of Cr/ZnO composites are relatively weak and broad attributed to the crystal deteriorations. No peaks related to chromium oxide phase or residual salt impurities are observed in the pattern referring to the high purity of the nanomaterials.<sup>17</sup> Furthermore, the close ionic radius of  $\text{Cr}^{3+}$  (0.063 nm) and  $\text{Zn}^{2+}$  (0.074 nm) as well as the small amount ratio of chromium ions led to easily substitution of  $\text{Zn}^{2+}$  with  $\text{Cr}^{3+}$  inside the host ZnO lattice. Only, a slide shift to higher  $2\theta$  angle was detected, resulting from the increase of strain and presence of defects.<sup>20–22</sup> The average crystallite size ( $D$ ) of the nanostructured materials was calculated by the Debye–Scherrer equation given by

$$D = \frac{k\lambda}{\beta \cos \theta} \quad (1)$$

where  $\beta$  is the full width at half-maximum,  $\theta$  is the Bragg's diffraction angle,  $\lambda$  is the wavelength of  $\text{CuK } \alpha = 1.5418 \text{ \AA}$ , and  $k$  is the crystallite shape factor = 0.94. By applying eq 1 on the sharp intense peak (101), the crystallite size was 31.32 and 26.25 nm for ZnO and Cr/ZnO-NPs, respectively. The dislocation density ( $\delta$ ) and lattice strain ( $\varepsilon$ ) were estimated from the following equations

$$\delta = \frac{1}{D^2} \quad (2)$$

and

$$\varepsilon = \frac{\beta}{4 \tan \theta} \quad (3)$$

The obtained values are summarized in Table 1. As presented,  $\delta$  and  $\varepsilon$  were increased, whereas  $D$  was decreased with  $\text{Cr}^{3+}$

**Table 1.** XRD Parameters of Un-doped and Cr-Doped ZnO NPs

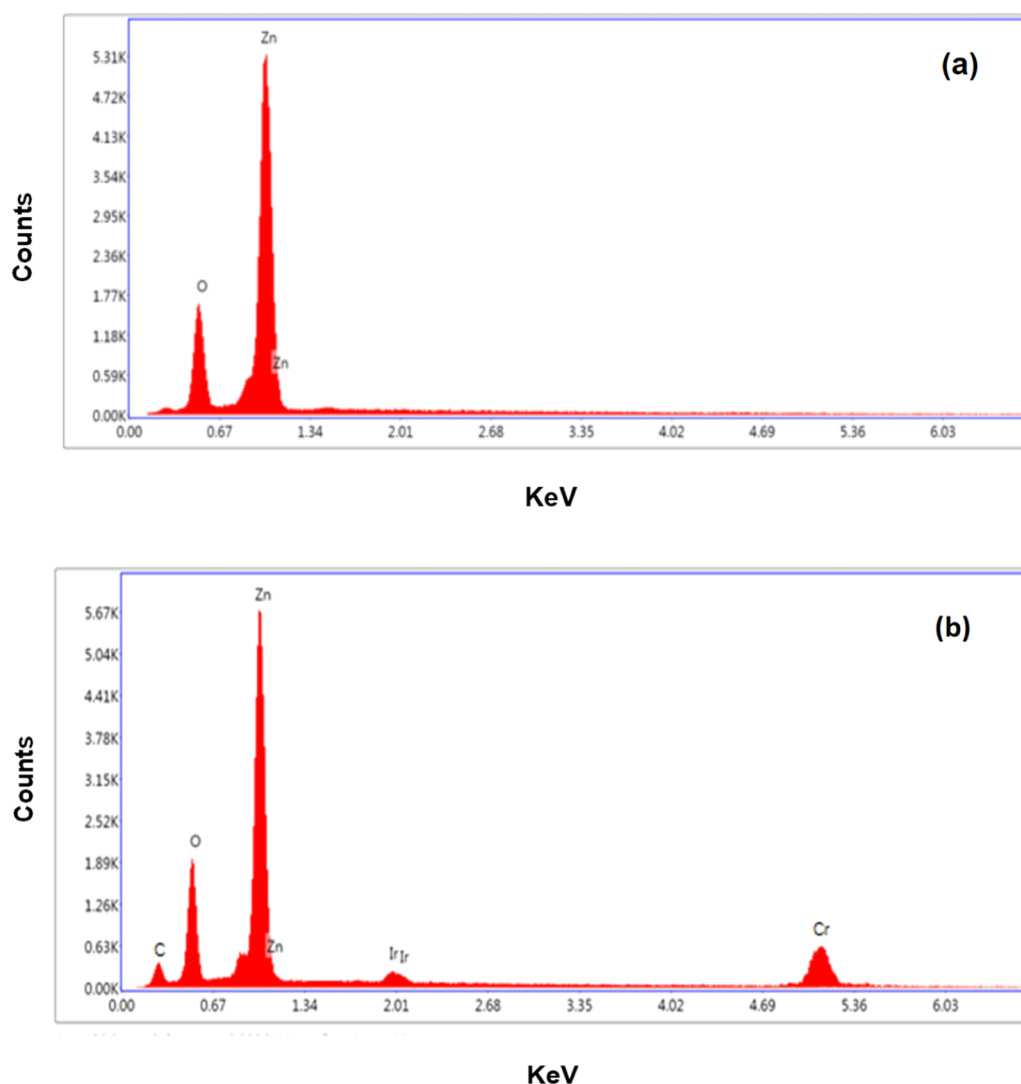
nanoparticles	$D$ (nm)	$\epsilon \times 10^{-4}$	$\delta \times 10^{-4} \text{ nm}^{-2}$
ZnO	31.34	44.05	9.30
Cr/ZnO	26.25	49.72	14.50

integration.<sup>23,24</sup> The crystal size reduction is related to the large-surface area and particle density. The chemical composition and purity of the NPs were investigated from the EDX spectra. As demonstrated in Figure 2a, the spectrum consists of Zn and O elements with weight percent (wt %) 62.08 and 37.92, respectively. Moreover, the EDX spectrum in Figure 2b has approved the incorporation of chromium ions inside the host framework forming Cr/ZnO-NPs. The weight percent of Zn, O, Cr, Ir, and C elements were 52.12, 21.55, 7.02, 8.42, and 10.89 wt %, respectively. The carbon peak was attributed to the carbon-coated grid while the Ir was associated with iridium vapor used for coating the samples.<sup>25,26</sup>

**3.1.2. TEM and AFM Micrographs.** The average size and particle distribution were examined by the TEM micrographs. Figure 3a describes the particles of ZnO in spherical shapes with high density and mean size  $\sim 34.70$  nm; however, some of

the NPs have a hexagonal shape. The particles of Cr/ZnO appear in a small particle size  $\sim 24.60$  nm with large surface-to-volume area, Figure 3b.<sup>27–29</sup> Furthermore, Figure 3c,d depicts the particle distribution with nanoscale size. To visualize the surface topological nature, 2D and 3D AFM micrographs were performed. As can be seen in Figure 4a,b, ZnO NPs have a round shape, uniformly grown and homogeneously distributed on the surface without voids. Figure 4c,d shows Cr/ZnO-NPs in clear tiny grains, uniformly distributed on the surface with high density. For further information, the SPIP program was utilized to define the surface roughness, porosity, and average size. The obtained results in Table 2 revealed that the particle size and surface roughness were decreased, whereas the porosity was increased with Cr<sup>3+</sup> concentration.<sup>30–32</sup> The results obtained from the TEM and AFM images clearly confirmed the particle size confinement with the doping support which is strongly matched with the XRD pattern. The structural–morphological results have revealed that Cr/ZnO-NPs possess unique characteristics, enabling them to be used in improvement of the electrode sensitivity.

**3.2. Optical Analysis of Un-doped and Cr-Doped Zinc Oxide Thin Films.** The optical properties of ZnO and Cr/ZnO thin films were investigated from transmittance ( $T$  %)

**Figure 2.** EDX spectra of (a) un-doped ZnO and (b) Cr-doped ZnO NPs.

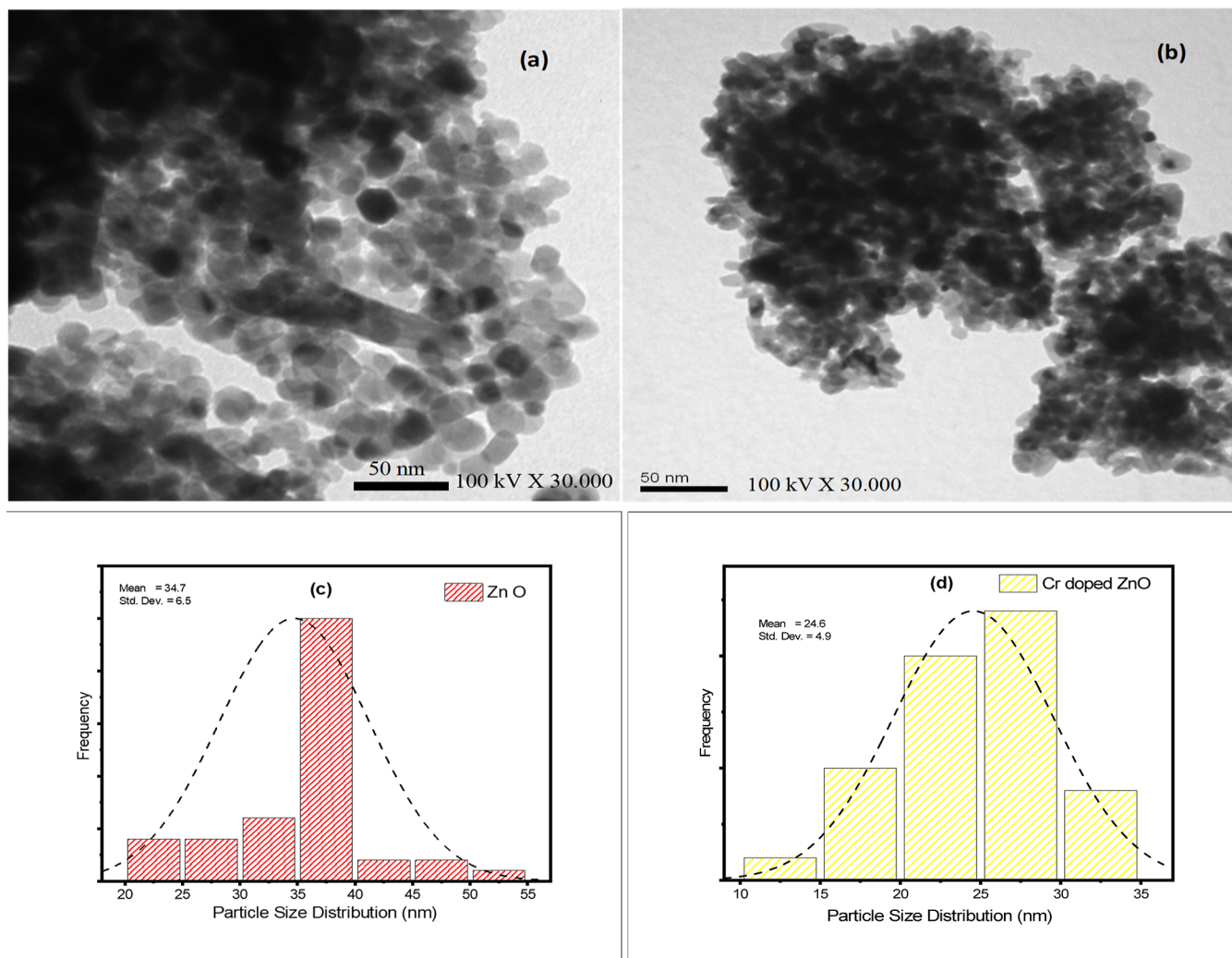


**Figure 3.** (a,b) TEM micrographs and (c,d) particle size distribution of un-doped ZnO and Cr doped ZnO NPs.

and reflectance ( $R$  %) spectra through the wavelength range from 300 to 800 nm. As illustrated in Figure 5a, ZnO NPs have good transparency and a strong absorption edge at 380 nm inside the visible spectrum. By adding chromium impurities, the optical transmission was drastically increased, resulting in shifting the fundamental absorption edge toward the ultraviolet (UV) region. Figure 5b shows the thin films of a wide reflectivity peak associated with the optical absorption and photon–electron interaction on the thin-film surface.<sup>21,22,33</sup> The absorption coefficient ( $\alpha$ ) was defined from  $T$  % and  $R$  % using the following relation

$$\alpha = \frac{1}{d} \ln \left[ \frac{(1 - R^2)}{2T} + \sqrt{\frac{(1 - R)}{4T^2} + R^2} \right] \quad (4)$$

where  $d$  is the film thickness of 782 and 640 nm for ZnO and Cr/ZnO, respectively. Figure 6a illustrates the absorption coefficient as a function of photon energy ( $h\nu$ ). The films revealed absorption peaks at approximately 3.55 eV attributed to the electron transition from valence band (VB) to conduction band (CB). The energy gap ( $E_g$ ) is an essential parameter used for identifying the optical transition of semiconductor materials from the Tauc equation<sup>34</sup>

$$\alpha = \frac{A}{h\nu} (h\nu - E_g)^n \quad (5)$$

Here,  $A$  is independent constant and  $n = 1/2$  for direct allowed transition. The energy gap was estimated by extrapolation of the straight line of  $(\alpha h\nu)^2 - (h\nu)$  Tauc graph at the energy axis = 0, Figure 6b. The  $E_g$  of ZnO was 3.75 eV expanded to 3.81 eV with  $\text{Cr}^{3+}$  contents. Another optical transition was observed in the range of 3.91–3.94 eV, suggesting the wide optical absorption. The blue-shift owing to the Burstein–Moss effect, by loading Cr ions inside the host ZnO lattice, trapped energy levels were generated inside the energy gap. According to Pauli principle, these extra donor levels result in transferring the electrons from the VB to higher energy levels of the CB.<sup>34,35</sup> The results obtained from the optical analysis coincide with the XRD data, where the disturbance in the ZnO lattice by doping led to quantum size confinement and hence crystalline size reduction.

**3.3. Electrodes Effective Surface Area.** For a concentration of 5 mM  $\text{K}_4\text{Fe}(\text{CN})_6$ , the surface area of the sensors was assessed using the CV method at various scan rates. The Randles–Sevcik equation describes the relationship between anodic peak current, scan rate, and the coefficient of diffusion of electro-active species which are abbreviated as  $I_{pa}$  ( $\mu\text{A}$ ),  $\nu$  ( $\text{Vs}^{-1}$ ), and  $D_o$  ( $\text{cm}^2 \text{s}^{-1}$ ), respectively. This equation is

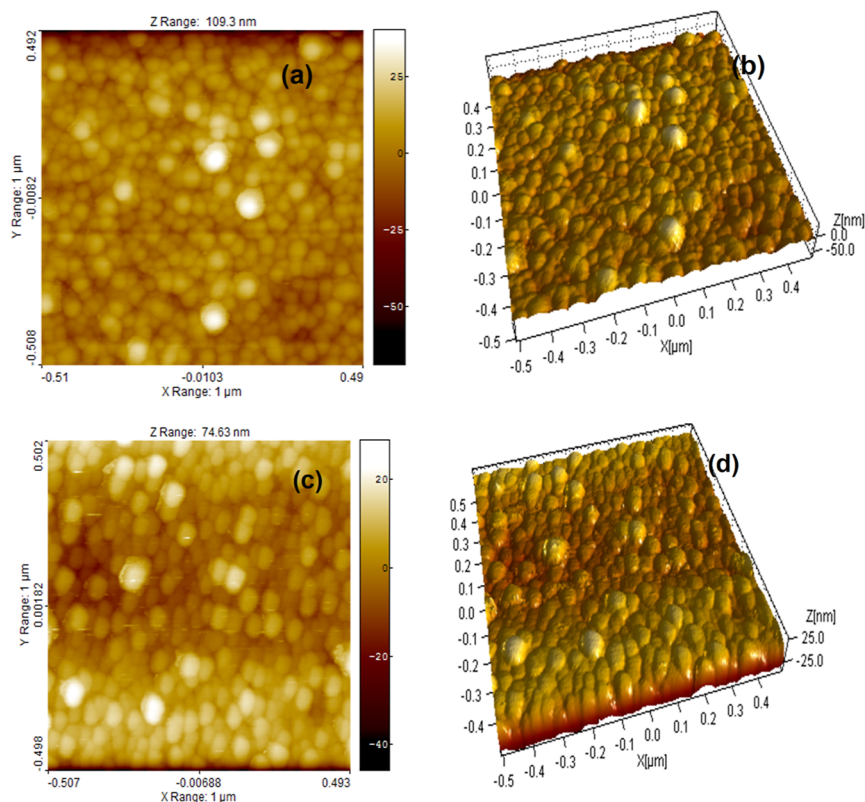


Figure 4. (2D and 3D) AFM of (a,b) ZnO and (c,d) Cr/ZnO-NP thin films.

Table 2. Topological Parameters of Un-doped and Cr-Doped ZnO Films Calculated from the AFM Images

nanoparticles	$D$ (nm)	surface roughness	porosity count
ZnO	28.60	10.30	72
Cr/ZnO	20.10	6.97	119

explained as:<sup>36</sup>  $I_p = (2.69 \times 10^5) n^{3/2} A_0 C_0 D_0^{1/2} v^{1/2}$ , where  $n$ ,  $A_0$ , and  $C_0$  symbolized to the number of electrons involved in the oxidation process, the electrode surface area, and the molar concentration of  $K_4Fe(CN)_6$ . In this instance,  $D_0 = 7.63 \times 10^{-6} \text{ cm}^2/\text{s}$ , and  $n = 1$ . The electroactive area of the introduced electrodes was computed after graphing the peak current versus square root of scan rate ( $v^{1/2}$ ), where the results acquired were 0.25, 0.096, and 0.054  $\text{cm}^2$  for 9% Cr/ZnO-NPs/CPE, ZnO/CPE, and CPE, respectively. In comparison to the other electrodes investigated, CPE with Cr/ZnO-NPs (7%, w/w) had the greatest electroactive surface area owing to the advantages of Cr/ZnO-NPs comprising the small particle size and large surface-to-volume area. Also, the strong optical absorption of the nanocomposite led to an increase in the free charge carriers on the electrode surface.

**3.4. ETF Electrochemical Performance.** The voltammetric performance of ETF in PBS buffer solution at pH 7, with a scan rate of 100 mV/s, exhibited just one oxidation signal in the forward direction with no reduction peak in the reverse scan (Figure 7). Anodic peak current was greater using Cr/ZnO-NPs/CPE compared to the non-modified CPE and ZnO/CPE. Besides, the sensitivity of electrode current was improved considerably due to the increased effective surface area and catalytic efficiency. The CPE was demonstrated due to its renewable surface that allows us to obtain reproducible results. The problems of electrode fouling are easily excluded

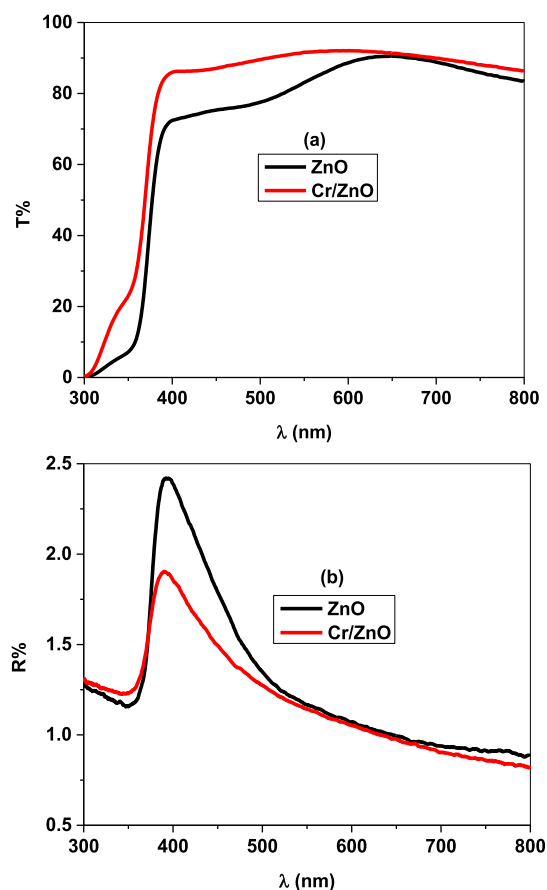
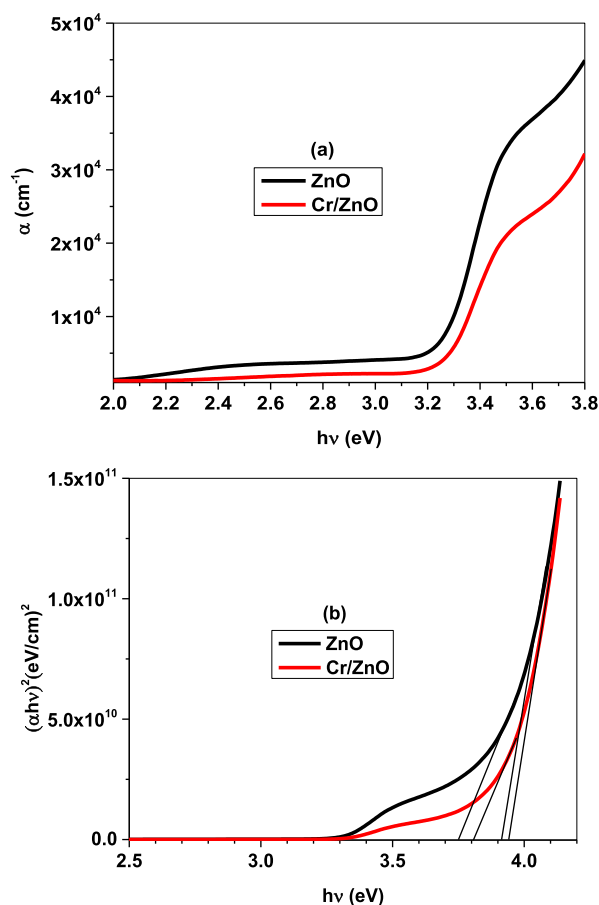
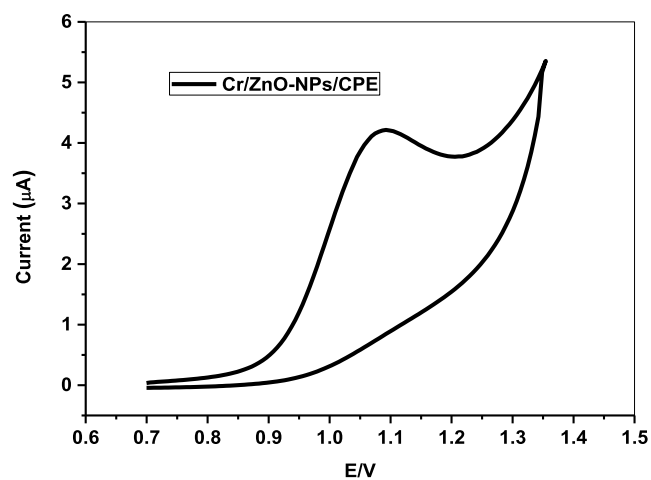


Figure 5. (a) Optical transmittance ( $T\%$ ) and (b) optical reflectance ( $R\%$ ) of the thin films.



**Figure 6.** (a) Optical absorption ( $\alpha$ ) as a function of ( $h\nu$ ) and (b) energy gap plot of ZnO and Cr/ZnO thin films.



**Figure 7.** Cyclic voltammogram of 100  $\mu\text{mol L}^{-1}$  ETF in PBS at pH 7, and a scan rate of 100 mV/s utilizing a Cr/ZnO-NPs/CPE.

by polishing the electrode between runs and hence obtaining highly reproducible results. The impact of percent contents of Cr/ZnO-NPs in the CPE was investigated, and the highest oxidation peak height for ETF was acquired at 7% w/w of Cr/ZnO-NPs, Figure 8a,b.<sup>36,37</sup> Here, the presence of chromium ions inside the ZnO framework results in the particle size confinement and hence increases the particles density on the surface as well as the chemical reactivity. Also, the high surface porosity played an important role in enhancement of the

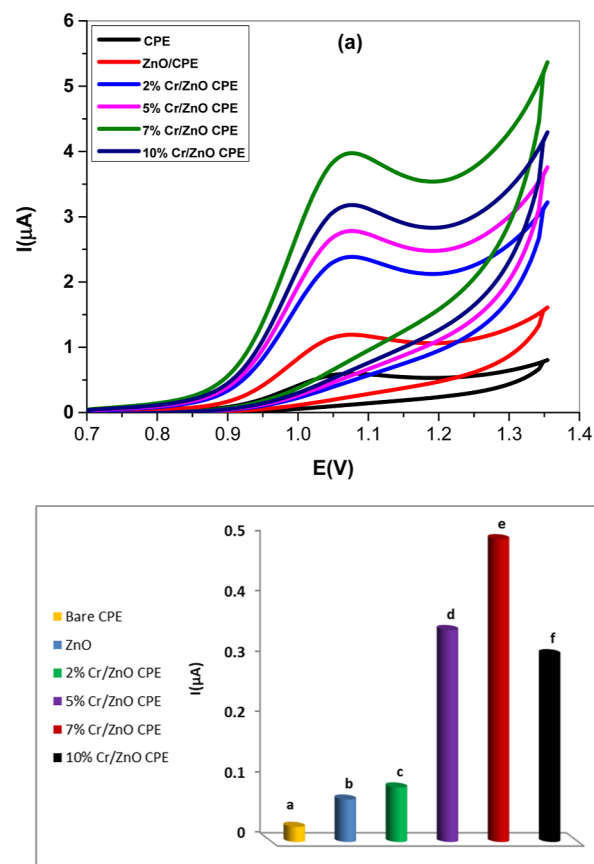


**Figure 8.** (a,b) Influence of Cr/ZnO-NPs/CPE percent content and several electrodes on 10  $\mu\text{mol L}^{-1}$ ETF peak height response employing SWV.

electrode efficacy. In addition to, the cyclic voltammograms were compared for the different electrodes.

**3.5. Optimization of the Voltammetric Method.** Three parameters, namely, the pH, buffer type, and scan rate, were investigated to improve the experimental conditions. Different buffers, including Britton Robinson, phosphate, acetate, borate, and citrate, were tested to obtain the best one, revealing the best-improved peaks. The PBS had the best peaks, but the others were lacking. The electro-oxidation behavior of ETF was also examined under varied pH and scan rate circumstances. It is important to note that the impact of temperature fluctuation on the performance of the electrochemical electrode sensor cannot be ignored. So, it is useful to fix the environmental temperature of the sensor using the temperature control system. In the current work, the temperature was adjusted at 20  $^{\circ}\text{C} \pm 2$ .

**3.5.1. Influence of pH.** The CV of 100  $\mu\text{mol L}^{-1}$  ETF was evaluated at the Cr/ZnO-NPs/CPE throughout a pH range of 3–10 of PBS to determine the effect of pH on ETF oxidation. The electrochemical irreversible oxidation of ETF displayed a prominent anodic peak at each pH, with currents dropping as pH raised, demonstrating that protons are implicated in the oxidation of ETF at the Cr/ZnO-NPs/CPE interface (Figure 9). Because the greatest peak current was seen at pH = 7, this value was chosen as the most optimal pH for future investigations and determination processes provided by PBS. The linear relationship between the peak potential and the pH of solution is seen in the equation below.



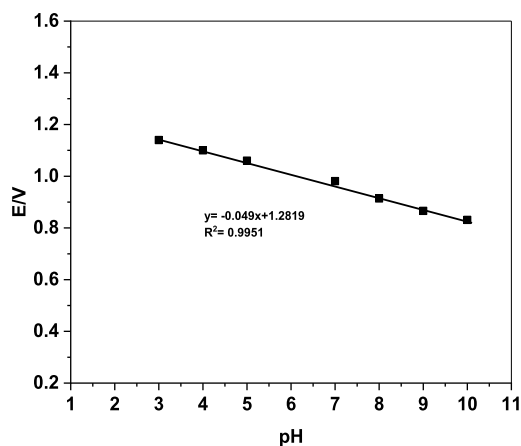


**Figure 9.** Influence of pH on 100  $\mu\text{mol L}^{-1}$  ETF peak current at the Cr/ZnO-NPs/CPE.

$$E(V) = -0.0452 \text{ pH} + 1.28$$

According to the resulting data of the previous equation, the electrode response slope is close to the Nernst equation ( $-0.059 \text{ mV/pH}$ ), revealing that the number of protons and electrons involved is the same. It was determined that the Cr/ZnO-NPs/CPE possess a greater intensity than plain CPE, ZnO where the highest current response and less positive overpotential shift at the Cr/ZnO-NPs/MNCT/CPE which related to the capability of Cr/ZnO-NPs to penetrate through the spacing between graphite layers of the CPE reaching the higher response using 7% w/w of Cr/ZnO-NPs, upon increase the Cr/ZnO-NPs will block the electrode surface to decrease the electrocatalytic activity.<sup>38,39</sup>

**3.5.2. Influence of the Scan Rate.** Scanning rate experiments were carried out to reveal if the electrochemical process was dominated by diffusion or adsorption or both. The influence of scan rates ( $\nu$ ) on peak current ( $I_p$ ) was investigated using the CV of ETF solution in PBS (pH 7). As shown in Figure 10b,  $\log I_p$  and  $\log \nu$  exhibited a linear relationship in the range of 0.02–0.18 V/s (Figure 10b), as given by the equation:

$$\log I_p (\mu\text{A}) = 0.537 \log \nu (\text{V/s}) + 1.137$$

The measured slope value (0.53) in above equation is close to the theoretically expected value (0.5) for the diffusion-controlled reaction, approving that ETF electro-oxidation is a diffusion-controlled process via the modified electrode (Cr/ZnO-NPs/CPE).<sup>38–40</sup> The cornerstone of the electrode sensing mechanism is a molecular diffusion process, which is described as the movement of molecules from a high concentration zone to a low concentration zone. The Laviron equation may be used to compute the number of electrons involved in an electrochemical reaction which is shown below

$$E = E^\circ + \left( \frac{2.303RT}{nF} \right) \log \left( \frac{RTK^\circ}{nF} \right) + \left( \frac{2.303RT}{nF} \right) \log \nu$$

Upon graphing the log scan rate ( $\log \nu$ ) versus potential (Figure 10a), the obtained slope can be used for  $\alpha n$  calculation. Where  $n$  is the number of electrons transferred and  $\alpha$  is the electron-transfer coefficient.

$$E_p (V) = 0.057 \log \nu + 1.114$$

The slope of the previous equation is 0.057, and  $\alpha n$  is 1.017. As a result of the irreversibility of ETF electro-oxidation,  $\alpha$  was said to be 0.5, and  $n$  was estimated to be  $\approx 2$ .

**3.6. Method Validation.** **3.6.1. Linearity, LOD, and LOQ.** The SWV technique was used to assess the linearity of the introduced method, where SWV was documented at different concentrations of ETF under optimum conditions. The calibration curve of peak current ( $I_p$ ) at different concentrations of pure ETF is shown in Figure 11. As shown, the anodic peak current ( $I_p, a$ ) is directly proportional to the ETF concentration based on the equation of  $I_p, a (\mu\text{A}) = 0.0305 C (\mu\text{g/mL}) + 0.1761$  ( $r = 0.9997$ ). The LOD and LOQ values were determined using the documented formulae in ICH guidelines which is based on the standard deviation of the calibration curve intercept (b) and the calibration curve slope (S). These formulae can be written as:  $\text{LOD} = 3.3 \text{ S/b}$  and  $\text{LOQ} = 10 \text{ S/b}$ .<sup>40,41</sup> Table 2 displays the values of the LOD and LOQ.

**3.6.2. Accuracy and Precision.** The preceding procedures of the suggested technique under linearity were accomplished three times for five various drug concentrations, in which the related regression equations were used to compute the concentrations. Table 3 demonstrates the mean % recoveries, which were examined and found to be adequate. The

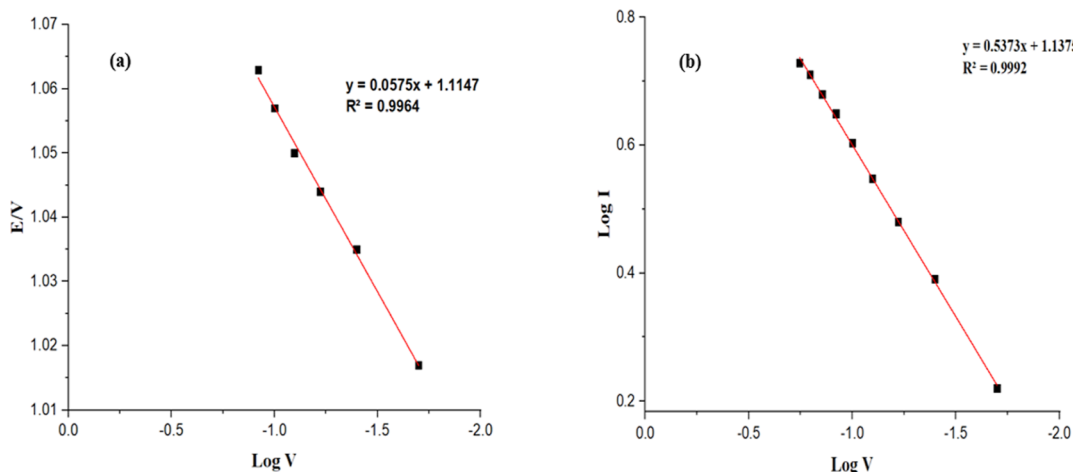


**Figure 10.** Log scan rate  $\nu$  versus (a) log oxidation current response  $I_p$  and (b) potential at the Cr/ZnO-NPs/CPE.

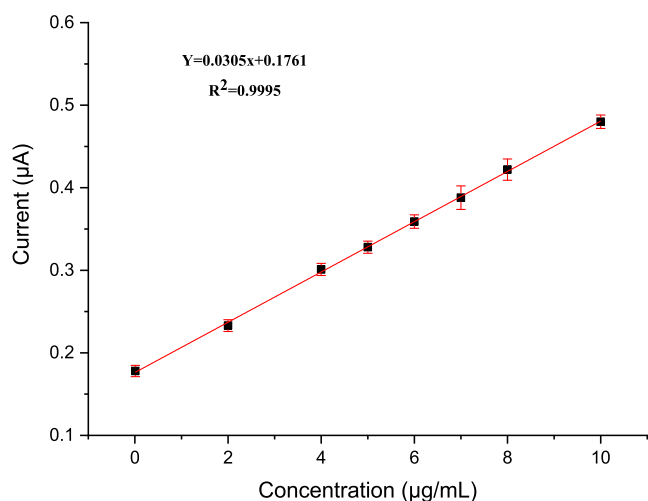


**Figure 11.** Calibration curve for the ETF ( $0.01\text{--}10\ \mu\text{mol L}^{-1}$ ) using a Cr/ZnO-NPs/CPE.

**Table 3. Validation Findings of the Introduced Method (SWV) for Quantification of ETF at Cr/ZnO-NPs/CPE**

parameters	SWV approach
linearity ( $\mu\text{mol L}^{-1}$ )	0.01–10
slope $\pm$ SD ( $\mu\text{mol L}^{-1}$ )	$0.444 \pm 0.001$
intercept $\pm$ SD	$0.563 \pm 0.033$
correlation coefficient ( $r$ )	0.9996
accuracy <sup>a</sup> (mean $\pm$ SD)	$99.67 \pm 0.745$
repeatability (% RSD)	0.876
intermediate precision <sup>b</sup> (% RSD)	0.986
LOD ( $\text{nmol L}^{-1}$ )	2.97
LOQ ( $\text{nmol L}^{-1}$ )	9

<sup>a</sup>Average of five measurements. <sup>b</sup>Average of three measurements.

repeatability and intermediate precisions were evaluated using percent relative standard deviation (% RSD) after assessing three various concentration levels within the linear range in triplicate in a single test run and in 3 successive days, respectively. The resultant percentage RSD values of less than 2 referred to the suggested method's accuracy and appropriateness for the assaying of ETF (Table 3).

**3.6.3. Reusability, Robustness, Reproducibility, and Stability.** The voltammetric output of the utilized sensor and the new one was compared to determine sensor reusability. The values from the two sensors were nearly similar, indicating that they may be reused. Robustness refers to the ability of an analytical technique to remain unchanged even if the approach was altered somewhat.<sup>41,42</sup> The robustness of the investigated approach was determined by studying two variables: equilibrium time ( $10 \pm 2\ \text{s}$ ) and pH variation ( $7 \pm 0.1$ ), where their influence on the peak current output was monitored. The peak current of ETF was unaffected by these minor changes that may occur during the experimental process, demonstrating the proposed method's robustness. Furthermore, the reproducibility of the estimated method was checked by fabricating five various Cr/ZnO-NPs/CPE sensors using the same conditions mentioned in heading 2.6. All the manufactured sensors produced virtually similar values, implying good reproducibility, demonstrated by a good RSD of 1.77.<sup>43</sup> The Cr/ZnO-NPs/CPE electrodes' day-to-day stability was estimated by determining the oxidation peak current at the concentration ( $0.04\ \mu\text{M}$ ) of ETF on the Cr/

ZnO-NPs/CPE over a period of 25 days. Furthermore, the Cr/ZnO-NPs/CPE electrodes were shown to have long-term stability after being kept in the refrigerator temperature for 25 days.

**3.6.4. Interference Experiment.** The presence of electroactive interfering materials in the same pharmaceutical formulation often causes systemic errors with ETF determination. Sensor selectivity could be checked by the interference experiment that depends on studying the influence of the addition of interferent analytes to the medium of ETF analysis. A combination of levodopa and ETF is effectively used for treating PD. Thus, we prepared four solutions comprising a constant concentration of levodopa ( $0.5\ \mu\text{mol L}^{-1}$ ) and variant ETF concentration ( $5\text{--}6\ \mu\text{mol L}^{-1}$ ) using PBS (pH 7). As shown in Figure 12, the SWV curves show a steady rise in ETF

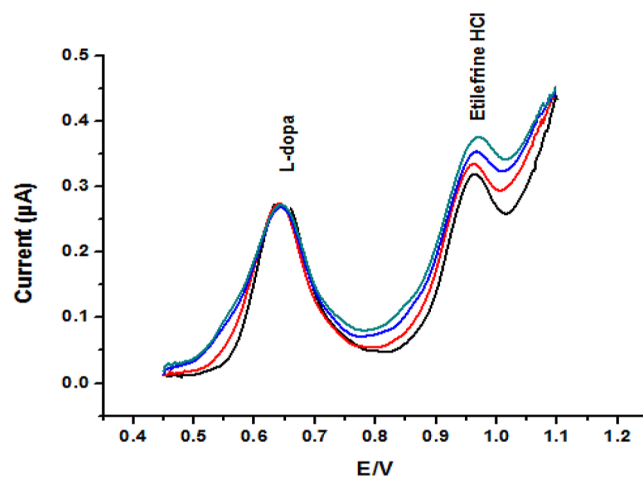


**Figure 12.** SWV of  $0.5\ \mu\text{mol L}^{-1}$  levodopa with different ETF concentrations ( $5\text{--}6\ \mu\text{mol L}^{-1}$ ) at the Cr/ZnO-NPs/CPE sensor in PBS (pH 7).

oxidation peak current compared to a constant levodopa concentration. This reflected the enhanced selectivity of the constructed sensor and exhibited the high resolution and precise quantification of the proposed approach.

**3.7. Application.** **3.7.1. Analysis of Marketable Dosage Form.** Due to the high selectivity of the suggested voltammetric approach, it had been successfully used to analyze the marketable dosage form. The analytical performance characteristics of the method were evaluated in two matrices to prove its efficiency and usefulness. Using the prepared Cr/ZnO-NPs/CPE sensor, SWV was effectively utilized to determine ETF in pharmaceutical formulation. According to Table 4, acceptable recovery rates (99.00–100.14%) were achieved. Recovery experiments were also conducted to verify the accuracy and precision of the designed approach using the multiple standard addition method. The validity of the suggested approach was further tested in an electrochemical cell by adding standard ETF produced in the supporting electrolyte and evaluating the analytical signals. According to the findings in Table 4, the suggested approach could adequately recover ETF in commercial pharmaceutical samples with no significant interference. Accordingly, the results indicated that the voltammetric method established with Cr/ZnO-NPs/CPE was scientifically valid in terms of accuracy and recovery.

**Table 4. Estimation of ETF in Marketed Tablets by SWV Using the Standard Addition Methodology**

marketed tablets	% found $\pm$ SD <sup>a</sup>	standard addition methodology		
		added ( $\mu\text{mol L}^{-1}$ )	found ( $\mu\text{mol L}^{-1}$ )	% recovery <sup>b</sup>
vascon labeled (5 mg/tab)	100.23 $\pm$ 0.67	0.1	0.099	99.00
		1.00	0.98	98.00
		3.00	2.98	99.33
		5.00	4.97	99.40
		7.00	7.01	100.14
			mean $\pm$ % RSD	

<sup>a</sup>Average of five measurements. <sup>b</sup>Average of three measurements.

**3.7.2. Analysis of ETF in Spiked Human Serum.** The ability of the prepared Cr/ZnO-NPs/CPE electrode for detecting ETF in complex matrix media such as human serum samples was investigated using the procedures described in heading 2.8. Validation parameters for the quantitative assessment of ETF in spiked human serum were determined utilizing the developed Cr/ZnO-NPs/CP electrode in PBS (pH 7), at a scan rate of 100 mV/s. As shown in Figure 13 and Table 5, the

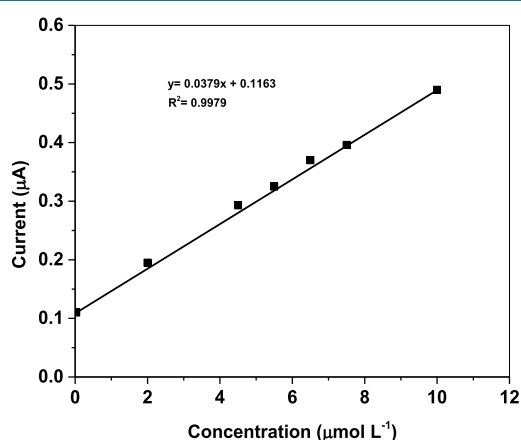


**Figure 13.** Serum calibration curve for ETF (0.05 to 10  $\mu\text{mol L}^{-1}$ ) using a Cr/ZnO-NPs/CPE.

**Table 5. Validation Parameters for Quantitative Assessment of ETF in Spiked Human Serum Utilizing the Developed Method**

parameters	human serum
linearity ( $\mu\text{mol L}^{-1}$ )	0.05–10
slope $\pm$ SD ( $\mu\text{mol L}^{-1}$ )	1.227 $\pm$ 0.005
intercept $\pm$ SD	1.331 $\pm$ 0.054
correlation coefficient ( <i>r</i> )	0.996
accuracy <sup>a</sup> (mean $\pm$ SD)	100.23 $\pm$ 0.521
LOD (nmol L <sup>-1</sup> )	13
LOQ (nmol L <sup>-1</sup> )	4

<sup>a</sup>Average of five measurements.

calibration curve showed a linear relationship in the range of 0.05–10  $\mu\text{mol L}^{-1}$ , with a correlation coefficient of 0.996 and a LOD of 13 nmol L<sup>-1</sup>. These findings revealed that the examined SWV approach can detect a wide range of ETF concentrations without interference from endogenous components that are often seen in human serum analysis.

**3.8. Statistical Comparison.** A comparison was made between the proposed method and the published potentiometric method.<sup>43,44</sup> As shown in Table 6, the computed values of Student's *t*-test and *F*-test were lower than the tabulated

**Table 6. Statistical Comparison of the Suggested and Reported Approaches for Analysis of ETF**

parameters	proposed method	reported method <sup>16</sup>
mean <sup>a</sup>	99.46	100.02
SD	1.129	0.779
variance	1.274	0.609
<i>n</i>	5	5
student's <i>t</i> -test	1.231 (2.306) <sup>b</sup>	
<i>F</i> -test	2.092 (6.39) <sup>b</sup>	

<sup>a</sup>Average of three measurements. <sup>b</sup>The parentheses indicate the theoretical values of *t* and *F* at *P* = 0.05.

ones, showing no notable change in accuracy and precision of the two methods. A one-way ANOVA with a 95% confidence interval (*P* = 0.05) was conducted to compare the recovery percentage for the developed electrodes and the reported potentiometric technique. As indicated in Table 7, the

**Table 7. ANOVA between Proposed Electrodes and Reported Method**

	sum of variations	sum of squares	degree of freedom	mean of squares	<i>F</i> -value	<i>P</i> -value	critical <i>F</i>
between group		1.116	3	0.372	0.394	0.758	3.238
within group		15.09	16	0.943			
total		16.21	19				

parameters of the ANOVA test revealed that the proposed approach had no statistically considerable differences from the reported potentiometric method, which validates the use of the developed methods.

**3.9. Method Greenness Profile Assessment.** The greenness evaluation of an analytical approach is critical to promoting environmental conservation. Numerous greenness assessment tools have recently been reported. The Eco-scale is an evaluation tool that handles the method's penalty points (PPs).<sup>45–47</sup> Several factors are used for calculating PP, including the quantity and quality of the materials, power consumption by the instruments, number of reagents utilized through the procedures, quantity of produced waste, and the safety of the analyst. Furthermore, the eco-scale score is determined as 100-PP after computing the overall PPs from the preceding four processes. As shown in Table 8, the ultimate score was 90, which was higher than 75, demonstrating the method's effectiveness in terms of long-term sustainability. Furthermore, the GAPI, which is a measure for evaluating the green character of an analytical methodology, was utilized to rate the greenness of the suggested voltammetric method. The GAPI protocol might be a useful semi-quantitative technique

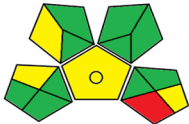
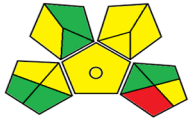
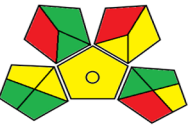

**Table 8. Penalty Points of the Developed Voltammetric Approach According to Analytical Eco-scale**

materials/equipments	PP of developed method	PP of reported method <sup>9</sup>	PP of reported method <sup>16</sup>	PP of reported method <sup>13</sup>
water	0	0	0	0
methanol		6		
hydrogen peroxide		6		6
phosphate buffer	1			1
Cr/ZnO-NPs/CPE	3			
phosphotungstic acid			3	
sodium tetra phenyl borate			2	
dioctyl phthalate			1	
poly vinyl chloride			2	
tetrahydrofuran			3	
acetonitrile				8
*occupational hazard instrument	0	0	0	0
energy ( $\leq 0.1$ kW h per sample)	0	0	0	1
waste	6	6	6	8
total number of penalty points	10	12	17	24
total eco-scale analysis	100 – 10 = 90	100 – 12 = 88	100 – 17 = 83	100 – 23 = 76

in laboratory work. The visual display of GAPI can be used for comparing different methods and selecting the most environmentally friendly approach for a certain investigation. In this tool, 15 parameters are evaluated for each stage in the analytical technique.

It describes the environmental impact of the analytical method using a color scale of three levels of low impact (green), medium impact (yellow), or high impact (red). As shown in Table 9, the proposed method exhibited high

**Table 9. Comparison of Suggested Voltammetric Method's Green Assessment Profile with Previously Published Methods, Utilizing GAPI Tool**

PP of developed method	
PP of Reported method [9]	
PP of Reported method [16]	
PP of Reported method [13]	

greenness level according to the GAPI standards. The green assessment profile of the suggested voltammetric method in comparison to four reported methods is shown in Tables 8 and 9.

#### 4. CONCLUSIONS

In the present study, un-doped and Cr-doped ZnO nanostructures were successfully prepared by a facile chemical co-precipitation approach. The crystallographic, morphological, and topological characteristics were investigated from XRD, EDX, TEM, and AFM measurements. The findings approved the impact of Cr<sup>3+</sup> dopants on the microstructure of ZnO, in which the particle size was decreased to ~26 nm while the porosity was significantly increased to 119. The optical analysis showed a blue-shift in the energy gap of ZnO with the dopant support. The superior physicochemical advantages comprising the quantum size effect and large-surface area-enabled Cr/ZnO-NPs to be used in fabricating a highly efficient electrode sensor. In the electrochemical investigations, the SWV approach was successfully used to quantify the ETF in a pure form, pharmaceutical formulations, and human serum. It was observed from the cyclic voltammogram that there was a significant irreversible anodic activity. Scanning rate experiments revealed the diffusion-regulated mass movement in the electrochemical process. The anodic peak current was linear under optimum circumstances for ETF concentrations, ranging from 0.01 to 10 mol L<sup>-1</sup>. The developed Cr/ZnO-NPs/CPE sensor has proven its efficiency in the determination of ETF in various matrices with satisfactory recovery. The validation of the SWV method involving Cr/ZnO-NPs/CPE sensors reflected the high-performance characteristics including high sensitivity, accuracy, linearity, good rapid static response, reasonable selectivity, and stability, with no risk of interference from excipients and its co-formulation drug. It is considered an environmentally friendly technique that does not require complex instruments or any separation stage, permitting ETF analysis without time-consuming and arduous procedures.

#### AUTHOR INFORMATION

##### Corresponding Author

Elsayed Elgazzar – Associate Professor of Physics, Physics Department, Faculty of Science, Suez Canal University, Ismailia 41511, Egypt; [orcid.org/0009-0009-9857-972X](https://orcid.org/0009-0009-9857-972X); Email: [elsayed.elgazzar@yahoo.com](mailto:elsayed.elgazzar@yahoo.com), [elsayed\\_mohsen@science.suez.edu.eg](mailto:elsayed_mohsen@science.suez.edu.eg)

## Authors

**Khadejah D. Otaif** – Department of Chemistry, Samtah University College, Jazan University, Jazan 86736, Saudi Arabia

**Manal M. Fouad** – Pharmaceutical Analytical Chemistry Department, Faculty of Pharmacy, October University for Modern Sciences and Arts (MSA), Giza 11787, Egypt

**Noha S. Rashed** – Pharmaceutical Analytical Chemistry Department, Faculty of Pharmacy (Girls), Al-Azhar University, Nasr City 11765 Cairo, Egypt

**Noha Y.Z. Hosni** – Pharmaceutical Analytical Chemistry Department, Faculty of Pharmacy (Girls), Al-Azhar University, Nasr City 11765 Cairo, Egypt

**Ahmed Elsonbaty** – Pharmaceutical Chemistry Department, Faculty of Pharmacy, Egyptian Russian University, Badr City 11829 Cairo, Egypt

Complete contact information is available at:

<https://pubs.acs.org/10.1021/acsomega.3c02381>

## Notes

The authors declare no competing financial interest.

## ACKNOWLEDGMENTS

The authors would like to thank both Jazan University, Saudi Arabia, and Suez Canal University, Egypt, for facilitating and supporting the research collaboration.

## REFERENCES

- (1) Ayad, M. M.; Abdellatef, H. E.; Hosny, M. M.; Kabil, N. A. S. Spectrophotometric determination of etilefrine HCl, salbutamol sulphate and tiemonium methyl sulphate using surface Plasmon resonance band of gold nanoparticles. *Nano Biomed. Eng.* **2018**, *10*, 16–24.
- (2) Attia, K. A. M.; El-Abasawy, N. M.; El-Olemy, A.; Abdel-Raouf, A. M. High Performance Liquid Chromatography Based on Computational Study for the Determination of Etilefrine Hydrochloride in the Presence of its Oxidative Degradation Product. *Anal. Chem. Lett.* **2016**, *6*, 457–469.
- (3) Srivastava, M.; Tiwari, P.; Mall, V. K.; Srivastava, S. K.; Prakash, R. Voltammetric determination of the antimalarial drug chloroquine using a glassy carbon electrode modified with reduced graphene oxide on WS<sub>2</sub> quantum dots. *Microchim. Acta* **2019**, *186*, 415.
- (4) Gomes Amorim, C.; Araújo, A.; da Conceição Montenegro, M. Use of cucurbit [6] uril as ionophore in ion selective electrodes for etilefrine determination in pharmaceuticals. *Electroanalysis* **2019**, *31*, 2171–2178.
- (5) El-Desoky, H. S.; Ghoneim, M. M.; Abdel-Galeil, M. M.; Habazy, A. D. Simple voltammetric method for nano estimation of etilefrine hydrochloride based on environmentally friendly montmorillonite natural clay. *J. Electrochem. Soc.* **2017**, *164*, H714–H725.
- (6) Veera Manohara Reddy, Y.; Bathinapatla, S.; Luczak, T.; Osinski, M.; Maseed, H.; Ragavendra, P.; Subramanyam Sarma, L.; Srikanth, V.; Madhavi, G. An ultra-sensitive electrochemical sensor for the detection of acetaminophen in the presence of etilefrine using bimetallic Pd–Ag/reduced graphene oxide nanocomposites. *New J. Chem.* **2018**, *42*, 3137–3146.
- (7) Venkateswarlu, S.; Venu, M.; Reddy, Y. V. M.; Sravani, B.; Mallikarjuna, K.; Yoon, M.; Madhavi, G. Facile Preparation of Ionic Liquid-coated Copper Nanowire-modified Carbon Paste Electrode for Electrochemical Detection of Etilefrine Drug. *Bull. Korean Chem. Soc.* **2019**, *40*, 560–565.
- (8) Mehmandoust, M.; Khoshnavaz, Y.; Tuzen, M.; Erk, N. Voltammetric sensor based on bimetallic nanocomposite for determination of favipiravir as an antiviral drug. *Microchim. Acta* **2021**, *188*, 434.
- (9) Chen, A.; Shah, B. Electrochemical sensing and biosensing based on square wave voltammetry. *Anal. Methods* **2013**, *5*, 2158.
- (10) Zamzam, N. S.; Hendawy, H. A. M.; Abdel-Raouf, A. M.; Abdelrahman, M. H. A Highly Sensitive Disposable In-House Screen-Printed Electrodes for Determination of 3, 5-di-tert-butyl-4-hydroxybenzoic Acid Aided by Essential Green Chemistry Tools: Application in Nile River Samples and Human Urine. *J. Electrochem. Soc.* **2021**, *168*, 117501.
- (11) Raymundo-Pereira, P. A.; Gomes, N. O.; Machado, S. A. S.; Oliveira, O. N., Jr. Wearable glove-embedded sensors for therapeutic drug monitoring in sweat for personalized medicine. *Chem. Eng. J.* **2022**, *435*, 135047.
- (12) Kelani, K. M.; Abdel-Raouf, A. M.; Ashmawy, A. M.; Omran, G. A.; Morshedy, S.; Wafaa Nassar, A. M.; Talaat, W.; Elgazzar, E. Electrochemical determination of dinitolmide in poultry product samples using a highly sensitive Mn<sub>2</sub>O<sub>3</sub>/MCNTs-NPs carbon paste electrode aided by greenness assessment tools. *Food Chem.* **2022**, *382*, 131702.
- (13) Verma, R.; Pathak, S.; Srivastava, A. K.; Praver, S.; Tomljenovic-Hanic, S. ZnO nanomaterials: Green synthesis, toxicity evaluation and new insights in biomedical applications. *J. Alloys Compd.* **2021**, *876*, 160175.
- (14) Martínez-Aguilar, E.; Hmök, H.; Herrera, O. R.; Betancourt, I.; López-Juárez, R. Structural, magnetic and polar effects in R-doped ZnO (R = Co, Cr, Cu and V): Study of first principles. *Mater. Chem. Phys.* **2022**, *279*, 125733.
- (15) Zeghoud, S.; Hemmami, H.; Ben Seghir, B.; Ben Amor, I.; Kouadri, I.; Rebiai, A.; Messaoudi, M.; Ahmed, S.; Pohl, P.; Simal-Gandara, J. A review on biogenic green synthesis of ZnO nanoparticles by plant biomass and their applications. *Mater. Today Commun.* **2022**, *33*, 104747.
- (16) Andolsi, Y.; Chaabouni, F. Optoelectronic properties of Cr doped ZnO thin films deposited by RF magnetron sputtering using a powder target. *J. Alloys Compd.* **2020**, *818*, 152739.
- (17) Chinnasamy, M.; Balasubramanian, K. Enhanced UV photo-detection behavior of Cr doped wurtzite ZnO crystalline nanorods. *Opt. Mater.* **2020**, *110*, 110492.
- (18) Debnath, T.; Chakraborty, T.; Bandyopadhyay, A.; Sharma, S.; Sinha Mahapatra, A.; Das, S.; Sutradhar, S. Modulation of structural, morphological and electrical charge transport property of Cr-doped ZnO nanomaterials prepared by chemical process. *Mater. Sci. Eng. B* **2022**, *280*, 115688.
- (19) Saraji, M.; Alijani, S. A molecularly imprinted polymer on chromium (III) oxide nanoparticles for spectrofluorometric detection of bisphenol A. *Spectrochim. Acta Mol. Biomol. Spectrosc.* **2021**, *255*, 119711.
- (20) Kumar, S.; Tiwari, N.; Jha, S. N.; Chatterjee, S.; Bhattacharyya, D.; Ghosh, A. K. Structural and optical properties of sol–gel derived Cr-doped ZnO diluted magnetic semiconductor nanocrystals: an EXAFS study to relate the local structure. *RSC Adv.* **2016**, *6*, 107816–107828. (n.d.)
- (21) Ashokkumar, M.; Muthusamy, C. Role of ionic radii and electronegativity of co-dopants (Co, Ni and Cr) on properties of Cu doped ZnO and evaluation of *In-vitro* cytotoxicity. *Surface. Interfac.* **2022**, *30*, 101968.
- (22) Rajivgandhi, G. N.; Ramachandran, G.; Alharbi, N. S.; Kadaikunnan, S.; Khaleed, J. M.; Manokaran, N.; Li, W.-J. Substantial effect of Cr doping on the antimicrobial activity of ZnO nanoparticles prepared by ultrasonication process. *Mater. Sci. Eng. B.* **2021**, *263*, 114817.
- (23) Srinet, G.; Sharma, S.; Guerrero-Sanchez, J.; Garcia-Diaz, R.; Ponce-Perez, R.; Siqueiros, J. M.; Raymond Herrera, O. Room-temperature ferromagnetism on ZnO nanoparticles doped with Cr: An experimental and theoretical analysis. *J. Alloys Compd.* **2020**, *849*, 156587.
- (24) Sharma, A.; Khangarot, R. K.; Misra, K. P.; Misra, R. D. K.; Chattopadhyay, S.; Babu, P. D.; Halder, N. Band gap reduction and quenching of pd exchange interaction in sol-gel derived Zn (Al, Cu) O nanostructures. *Phys. Scr.* **2021**, *96*, 075803.

- (25) Pandey, P. K.; Chauhan, V.; Dixit, P.; Pandey, P. C. Correlation of enhanced photocurrent with structural and optical properties of Ag–ZnO nanocomposites synthesized by a facile chemical route. *Phys. B Condens. Matter*. **2021**, *612*, 412937.
- (26) Namini, A. S.; Delbari, S. A.; Mousavi, M.; Ghasemi, J. B. Synthesis and characterization of novel ZnO/NiCr<sub>2</sub>O<sub>4</sub> nanocomposite for water purification by degradation of tetracycline and phenol under visible light irradiation. *Mater. Res. Bull.* **2021**, *139*, 111247.
- (27) Sagheer, R.; Khadija, S. T.; Kayani, Z. N.; Riaz, S. Structural, optical and magnetic properties of ZnO nanoparticles tailored by 'La<sup>3+</sup>' ions. *Optik—International Journal for Light and Electron Optics* **2021**, *244*, 166816.
- (28) Ghotekar, S.; Pansambal, S.; Bilal, M.; Pingale, S. S.; Oza, R. Environmentally friendly synthesis of Cr<sub>2</sub>O<sub>3</sub> nanoparticles: characterization, applications and future perspective— a review. *Case Stud. Chem. Environ. Eng.* **2021**, *3*, 100089.
- (29) Prabakar, C.; Muthukumar, S.; Raja, V. Influence of defects on the structural, optical, photoluminescence and magnetic properties of Cr/Mn dual doped ZnO nanostructures. *Chemical Physics Impact* **2021**, *2*, 100019.
- (30) Matos, R. S.; Attah-Baah, J. M.; Monteiro, M. D. S.; Costa, B. F. O.; Mácado, M. A.; Silva Junior, R. S.; da Fonseca Filho, H. D.; Oliveira, R. M. P. B.; Ferreira, N. S. Effect of the amapa-latex chelating agent contents on the microstructure and photocatalytic properties of ZnO nanoparticles. *J. Mater. Res. Technol.* **2023**, *22*, 2673–2689.
- (31) Yu, M.; Yang, L.; Yan, L.; Wang, T.; Wang, Y.; Qin, Y.; Xiong, L.; Shi, R.; Sun, Q. ZnO nanoparticles coated and stearic acid modified superhydrophobic chitosan film for self-cleaning and oil–water separation. *Int. J. Biol. Macromol.* **2023**, *231*, 123293.
- (32) Gunduz, B.; Al-Ghamdi, A. A.; Hendi, A. A.; Gafer, Z. H.; El-Gazzar, S.; El-Tantawy, F.; Yakuphanoglu, F. New Schottky diode based entirely on nickel aluminate spinel/p-silicon using the sol–gel spin coating approach. *Superlattices Microstruct.* **2013**, *64*, 167–177.
- (33) Bonyadi, S.; Ghanbari, Kh. Application of molecularly imprinted polymer and ZnO nanoparticles as a novel electrochemical sensor for tartrazine determination. *Microchem. J.* **2023**, *187*, 108398.
- (34) Tiwari, A.; Sahay, P. P. Sn-Ga co-doping in sol-gel derived ZnO thin films: studies of their microstructural, optical, luminescence and electrical properties. *Mater. Sci. Semicond. Process.* **2020**, *118*, 105178.
- (35) Nakarungsee, P.; Srirattanapibul, S.; Issro, C.; Tang, I.-M.; Thongmee, S. High performance Cr doped ZnO by UV for NH<sub>3</sub> gas sensor. *Sens. Actuators, A* **2020**, *314*, 112230.
- (36) Sharma, H. K.; Archana, R.; Sankar ganesh, R.; Singh, B. P.; Ponnusamy, S.; Hayakawa, Y.; Muthamizhchelvan, C.; Raji, P.; Kim, D. Y.; Sharma, S. K. Substitution of Al<sup>3+</sup> to Zn<sup>2+</sup> sites of ZnO enhanced the photocatalytic degradation of methylene blue under irradiation of visible light. *Solid State Sci.* **2019**, *94*, 45–53.
- (37) Ghanbari Shohany, B.; Khorsand Zak, A. Doped ZnO nanostructures with selected elements - Structural, morphology and optical properties: A review. *Ceram. Int.* **2020**, *46*, 5507–5520.
- (38) Ali, M. B.; Abdel-Raouf, A. M.; Hendawy, H. A. M.; Talaat, W.; Omran, G. A.; Morshedy, S. An Eco-Friendly Solid-State Electrode Modified With ZnO Nanoparticles Decorated With MWCNT as an Electrochemical Sensor for the Determination of Avanafil in Pure Form, Dosage Form and Human Plasma. *J. Electrochem. Soc.* **2021**, *168*, 087510.
- (39) Abdallah, O. M.; Mohamed, T. A.; Hendawy, H.; Elomda, H. Voltammetric method for determination of Palonosetron Hydrochloride in the presence of its degradant using synergistic effect of ZnO nanoparticles and carbon nanotubes in micellar media. *Egypt J. Chem.* **2022**, *65*, 597.
- (40) Abdel-Raouf, A. M.; Osman, A. O. E.; El-Desouky, E. A.; Abdel-Fattah, A.; Abdul-Kareem, R. F.; Elgazzar, E. Fabrication of an (α-Mn<sub>2</sub>O<sub>3</sub>:Co)-decorated CNT highly sensitive screen printed electrode for the optimization and electrochemical determination of cyclobenzaprine hydrochloride using response surface methodology. *RSC Adv.* **2020**, *10*, 24985–24993.
- (41) Abdel-Atty, S.; Abdel-Raouf, A. M.; Mohamed, T. F.; Nasr, Z. A.; Mohamed, G. F.; Elgazzar, E. The Fabrication of a Highly Sensitive Nano Green Carbon Paste Electrode Modified with Yttrium Doped Manganese Oxide (Mn<sub>2</sub>O<sub>3</sub>/Y<sub>2</sub>O<sub>3</sub>) for Electrochemical Determination of Marbofloxacin and Its Residues in Bovine Meat and Milk Samples. *J. Electrochem. Soc.* **2020**, *167*, 107509.
- (42) Raymundo-Pereira, P. A.; Lima, A. R. F.; Machado, S. A. S. A nanostructured label-free platform based on an ultrathin film for ultrasensitive detection of a secosteroid hormone. *RSC Adv.* **2016**, *6*, 34458–34467.
- (43) Koçak, B.; İpek, Y.; Keçeci, A. A novel electrochemical sensor for metoprolol analysis based on glutardialdehyde–zinc oxide modified boron doped diamond electrode. *Diam. Relat. Mater.* **2023**, *131*, 109558.
- (44) Naeemy, A.; Sedighi, E.; Mohammadi, A. Electrooxidation of zolpidem and its voltammetric quantification in standard and pharmaceutical formulation using pencil graphite electrode. *J. Electrochem. Sci. Technol.* **2016**, *7*, 68–75.
- (45) Silva, M.; Morante-Zarcelero, S.; Pérez-Quintanilla, D.; Sierra, I. Simultaneous determination of pindolol, acebutolol and metoprolol in waters by differential-pulse voltammetry using an efficient sensor based on carbon paste electrode modified with amino-functionalized mesostructured silica. *Sens. Actuators B Chem.* **2019**, *283*, 434–442.
- (46) Ferreira, H.; Conradie, M. M.; Conradie, J. Redox behaviour of imino-β-diketonato ligands and their rhodium (I) complexes. *Results Chem* **2022**, *4*, 100517.
- (47) Song, Y.-S.; Dai, M.-Z.; Zhu, C.-X.; Huang, Y.-F.; Liu, J.; Zhang, C.-D.; Xie, F.; Peng, Y.; Zhang, Y.; Li, C.-Q.; et al. Validation, optimization, and application of the zebrafish developmental toxicity assay for pharmaceuticals under the ICH S5 (R3) guideline. *Front. Cell Dev. Biol.* **2021**, *9*, 721130.

## Recommended by ACS

### Study on Nitrogen Injection Fire Prevention and Extinguishing Technology in Spontaneous Combustion Gob Based on Gob-Side Entry Retaining

Xihua Zhou, Gang Bai, et al.

AUGUST 10, 2023  
ACS OMEGA

READ 

### Cooling of a PVT System Using an Underground Heat Exchanger: An Experimental Study

Saif H. Majeed, Wan Nor Roslam Wan Isahak, et al.

AUGUST 08, 2023  
ACS OMEGA

READ 

### Comparative Analysis of Metabolic Compositions and Trace Elements of *Ornithogalum caudatum* with Different Growth Years

Xueliang Zhao, Yang Xu, et al.

JUNE 21, 2023  
ACS OMEGA

READ 

### Study on Slagging Characteristics of Boiler Pre-combustion Chambers Based on Deep Learning

Bo Zhang, Zixian Huo, et al.

APRIL 19, 2023  
ACS OMEGA

READ 

Get More Suggestions >